

Analysis of the transversely isotropy, due to the production process, of carbon black filled SBR

Gianfilippo Dottore
Department of Civil Engineering and Architecture
University of Catania (*Italy*)
email: gianfilippo.dottore@gmail.com

Abstract—Through tensile tests of uniaxial and planar type, was proceeded to the mechanical characterization of SBR rubber sheets filled with particles of carbon black. The analysis has allowed defining the elastic features, the storage modulus, the transversal contraction coefficient (both obtained from uniaxial testing) and the shear modulus (from the planar/pure shear tests). Due to the calendering process by which was obtained, the elastomer sheet it's shown transversely isotropic, with different mechanical behavior in the direction of processing with respect to the transverse direction. Therefore, it was essential to evaluate two different values for each storage modulus, depending that the sample was loaded in the direction of calendering or in that orthogonal to it.

Index Terms—Transversal Isotropy, Hyperelasticity, SBR, Carbon Black, Calendering.

I. INTRODUCTION

The Styrene Butadiene Rubber (SBR) arises from copolymerization of Butadiene and Styrene. The latter, present to the extent of 20-25% of the copolymer, increases both strength and stiffness from SBR with respect to the butadiene rubber (BR) [1], [2]. Often, it is filled with carbon black, carbon charges of nanometric particles obtained from the combustion of hydrocarbons, the presence of which improves the mechanical properties and slows the aging. The SBR is the most usage rubber [3], [4], [5], [6], [7], [8], [9], being able to provide mechanical properties similar to those of natural rubber at a lower cost. The elastomer is used mainly where there is a need for high-friction surfaces, so that the 70% of the production is for tires tread [10], [11], [12], [13].

The mechanical characterization of a material consists in determining the current constitutive law between stress and strain [3], [14], [15], [16].

The characterization process is particularly critical for elastomers, due the large deformations that, for the same elastomer definition [17], [18], can tolerate without reaching the failure.

The aim of this experimental analysis is reached the mechanical characterization of styrene-butadiene rubber, improved in its quality by the introduction of fillers of carbon black (25%) in the blend [4], [19].

The analysis developed is focused on tracking of mathematical functions, which correlated stress and strain, and on evaluation, starting with these functions, of the storage modules assumed at the beginning of the rubber test.

Transversely isotropic behavior, caused by the rubber calendering process [20], has made more difficult the analysis. The phenomenon is well known in the literature, so that were already made attempts to characterize elastomers which have transverse isotropy [21], [22], [23].

Therefore, tests were performed at different loading directions, in order to assess the behavioral differences of the material between the direction of calendering and the direction orthogonal to it.

II. CONSTITUTIVE EQUATIONS

Most of engineering materials belongs to the category of simple materials, for which the stress tensor \mathbf{T} is a function of the history of the position gradient $F = \nabla x$ [2]:

$$T(x, t) = T(F(x, \tau), x_0, t) \quad \tau \in [0, t] \quad (1)$$

Among the simple materials, those elastic exhibit a stress state as a function of the single value of the deformation gradient:

$$T(x, t) = T(F(x, \tau), x_0, t) \quad (2)$$

According to this constitutive relationship, stress does not depend on the deformation path (Cauchy elasticity), but it is not the same for the deformation work that it performs. The *hyperelastic* materials are, instead, conservative elastic materials (Green elasticity), i.e. for which, there being an elastic potential function $\varphi = \varphi(\mathbf{F})$, which can be derived from stress, the differential form of the deformation work is exact

$$\left(\frac{\partial \varphi}{\partial \mathbf{F}} \right)^t = \mathbf{T}_I \quad (3)$$

where $\mathbf{T}_I := J\mathbf{T}\mathbf{F}^{-t}$ is the *first tensor of Piola-Kirchhoff*, with $J = \det \mathbf{F}$.

The simple assumption of linear elastic material is correct if you can overlook the time-dependent effects (such as sliding and relaxation) [2], [24], [25] and for small deformations. Circumstance, the latter, in which it is allowed the stress-strain relationship linearization. The linear stress-strain law is represented in classic form, tensorial, from equations $T_{ij} = \sum_{h,k=1}^3 C_{ijhk} E_{hk}$, which contain the $3^4 = 81$ constants C_{ijhk} of the elastic tensor di of order 4. Since the stress and strain

symmetry of the tensors requires six independent components of the stress tensor as a function of the six independent components of the strain tensor, only 36 independent constants are needed to determine the linear elastic relationship.

$$[\sigma] := \begin{bmatrix} \sigma_x \\ \sigma_y \\ \sigma_z \\ \tau_{xy} \\ \tau_{xz} \\ \tau_{yz} \end{bmatrix} = \begin{bmatrix} \sigma(1) \\ \sigma(2) \\ \sigma(3) \\ \sigma(4) \\ \sigma(5) \\ \sigma(6) \end{bmatrix}; \quad [\dot{\varepsilon}] := \begin{bmatrix} \dot{\varepsilon}_x \\ \dot{\varepsilon}_y \\ \dot{\varepsilon}_z \\ \dot{\gamma}_{xy} \\ \dot{\gamma}_{xz} \\ \dot{\gamma}_{yz} \end{bmatrix} = \begin{bmatrix} \dot{\varepsilon}(1) \\ \dot{\varepsilon}(2) \\ \dot{\varepsilon}(3) \\ \dot{\varepsilon}(4) \\ \dot{\varepsilon}(5) \\ \dot{\varepsilon}(6) \end{bmatrix}$$

We can express the linear relationship in a matrix simplified using independent components vectors

$$\begin{bmatrix} \sigma_x \\ \sigma_y \\ \sigma_z \\ \tau_{xy} \\ \tau_{xz} \\ \tau_{yz} \end{bmatrix} = \begin{bmatrix} c_{11} & c_{12} & c_{13} & c_{14} & c_{15} & c_{16} \\ c_{21} & c_{22} & c_{23} & c_{24} & c_{25} & c_{26} \\ c_{31} & c_{32} & c_{33} & c_{34} & c_{35} & c_{36} \\ c_{41} & c_{42} & c_{43} & c_{44} & c_{45} & c_{46} \\ c_{51} & c_{52} & c_{53} & c_{54} & c_{55} & c_{56} \\ c_{61} & c_{62} & c_{63} & c_{64} & c_{65} & c_{66} \end{bmatrix} \begin{bmatrix} \varepsilon_x \\ \varepsilon_y \\ \varepsilon_z \\ \gamma_{xy} \\ \gamma_{xz} \\ \gamma_{yz} \end{bmatrix}$$

The linear elastic relationship is defined by $6 \times 6 = 36$ components of the \mathbf{C} tensor of order 2 of elastic constants. Assuming the occurrence of a potential elastic (hyperelastic material), according to the Schwartz theorem, the elasticity tensors are symmetrical and the constants are reduced to 21 [3].

They are called *transversely isotropic* those materials, which have an isotropic response in the plane orthogonal to an axis, said *axis of transverse symmetry*. By choosing a base having the x-axis parallel to symmetry transverse

$$\begin{bmatrix} \sigma_x \\ \sigma_y \\ \sigma_z \\ \tau_{xy} \\ \tau_{xz} \\ \tau_{yz} \end{bmatrix} = \begin{bmatrix} c_{11} & c_{12} & c_{13} & 0 & 0 & 0 \\ c_{12} & c_{22} & c_{23} & 0 & 0 & 0 \\ c_{13} & c_{23} & c_{33} & 0 & 0 & 0 \\ 0 & 0 & 0 & c_{44} & 0 & 0 \\ 0 & 0 & 0 & 0 & c_{44} & 0 \\ 0 & 0 & 0 & 0 & 0 & \frac{c_{22}-c_{23}}{2} \end{bmatrix} \begin{bmatrix} \varepsilon_x \\ \varepsilon_y \\ \varepsilon_z \\ \gamma_{xy} \\ \gamma_{xz} \\ \gamma_{yz} \end{bmatrix}$$

In this case, the elastic response is described by 5 independent parameters [26].

The constitutive equation can be formulated in terms of engineering constants [3], inverting the stress-strain relation

$$\begin{bmatrix} \varepsilon_x \\ \varepsilon_y \\ \varepsilon_z \\ \gamma_{xz} \\ \gamma_{xz} \\ \gamma_{yz} \end{bmatrix} = \mathbf{C}^{-1} \begin{bmatrix} \sigma_x \\ \sigma_y \\ \sigma_z \\ \tau_{xy} \\ \tau_{xz} \\ \tau_{yz} \end{bmatrix}$$

and

$$\mathbf{C}^{-1} = \begin{bmatrix} \frac{1}{E_x} & -\frac{\nu_{xy}}{E_y} & -\frac{\nu_{xy}}{E_y} & 0 & 0 & 0 \\ -\frac{\nu_{yx}}{E_x} & \frac{1}{E_y} & -\frac{\nu_{yz}}{E_y} & 0 & 0 & 0 \\ -\frac{\nu_{yx}}{E_x} & -\frac{\nu_{yz}}{E_y} & \frac{1}{E_y} & 0 & 0 & 0 \\ 0 & 0 & 0 & 1/G_{xy} & 0 & 0 \\ 0 & 0 & 0 & 0 & 1/G_{xy} & 0 \\ 0 & 0 & 0 & 0 & 0 & \frac{2(1+\nu_{yz})}{E_y} \end{bmatrix}$$

where the 6 modules present are defined as follows

$$E_i = \frac{\sigma_i}{\varepsilon_i} \quad \sigma_{(i)} \neq 0, \quad \sigma_{(k)} = 0 \quad \forall k \neq i$$

$$G_{ij} = \frac{\tau_{ij}}{\gamma_{ij}} \quad \sigma_{(i)} \neq 0, \quad \sigma_{(k)} = 0 \quad \forall k \neq i$$

$$G_{ij} = \frac{\tau_{ij}}{\gamma_{ij}}$$

The elements on the main diagonal are the modules of normal deformability $1/E_i$ and tangential $1/G_{ij}$; those that appear outside of the same diagonal such as the modules of transverse deformability $-\nu_{ji}/E_i$. The symmetry of the previous matrix adds the condition $\nu_{yx}/E_x = \nu_{xy}/E_y$, which reduces to 5 the independent components. In the case of transversely isotropic material plates, which present the x or y axis of transverse symmetry, assuming the status of plane stress $\sigma_z = \tau_{xz} = \tau_{yz} = 0$ and writing separately the equations:

$$\varepsilon_z = -\frac{\nu_{yx}}{E_x} \sigma_x + \frac{1}{E_y} (\sigma_z - \nu_{yz} \sigma_y)$$

$$\gamma_{xz} = 0$$

$$\gamma_{yz} = 0$$

the constitutive relation can be narrowed to only three stress and three strain components in the x and y directions, becoming [27], [3]:

$$\begin{bmatrix} \sigma_x \\ \sigma_y \\ \tau_{xy} \end{bmatrix} = \begin{bmatrix} \frac{E_x}{1-\nu_{xy}\nu_{yx}} & \frac{\nu_{xy}E_x}{1-\nu_{xy}\nu_{yx}} & 0 \\ \frac{\nu_{yx}E_y}{1-\nu_{xy}\nu_{yx}} & \frac{E_y}{1-\nu_{xy}\nu_{yx}} & 0 \\ 0 & 0 & G_{xy} \end{bmatrix} = \begin{bmatrix} \varepsilon_x \\ \varepsilon_y \\ \gamma_{xy} \end{bmatrix}$$

$$\begin{bmatrix} \varepsilon_x \\ \varepsilon_y \\ \gamma_{xy} \end{bmatrix} = \begin{bmatrix} \frac{1}{E_x} & -\frac{\nu_{xy}}{E_y} & 0 \\ \frac{\nu_{yx}}{E_x} & \frac{1}{E_y} & 0 \\ 0 & 0 & \frac{1}{G_{xy}} \end{bmatrix} = \begin{bmatrix} \sigma_x \\ \sigma_y \\ \tau_{xy} \end{bmatrix}$$

where there is a symmetry condition $\nu_{yx}/E_x = \nu_{xy}/E_y$, whose effect is that only 4 of the 5 elastic constants appearing in the above matrix are independent.

III. PURE SHEAR IN PLANAR TEST

A valid constitutive model must properly describe the material behavior for each stress state. A single test as a simple uniaxial tensile test does not allow the construction of a reliable model in every situation. It then requires the programming of tests set that provide different stress mode. The uniaxial tensile test is then flanked by planar tensile and equibiaxial tests [4], [19].

The planar tensile test replaces the pure shear test (torsion of cylindrical sample), not applicable on samples cut from rubber sheets. The central portion of the specimen is subject to a pure shear strain and stress [4], [24]. To prove this assumption, we consider an orthogonal axes system, formed by the loading direction, from the direction perpendicular to this plane in the specimen and the direction normal to the sample itself. Noted these directions, respectively, with the letters x , y , z (Fig. 1, 2):

The test consists to creating a stretching in the x -direction. For implementation of the test (high ratio width/length of the sample), it is considered negligible the strain along the y -direction

$$\lambda_y = 1 \Rightarrow \dot{\epsilon}_y = 0$$

Consequently, the incompressibility condition $J = \det \mathbf{F} = 1 \Rightarrow \dot{\epsilon}_V = \dot{\epsilon}_x + \dot{\epsilon}_y + \dot{\epsilon}_z = 0$ for planar test is written [2]:

$$J = \lambda_x \lambda_z \Leftrightarrow 1 \Rightarrow \lambda_z = \frac{1}{\lambda_x}$$

$$\dot{\epsilon}_V = \dot{\epsilon}_x + \dot{\epsilon}_z \Leftrightarrow \dot{\epsilon}_z = -\dot{\epsilon}_x$$

Therefore, assuming the incompressibility of the material, the coordinates of tensors \mathbf{F} and $\mathbf{V} = 1/2(\text{grad } \mathbf{v} + \text{grad } \mathbf{v}^t)$ (strain rate) respect to the system of axes x , y , z are.,

$$[\mathbf{F}]_{xyz} = [\mathbf{F}_D]_{xyz} = \begin{bmatrix} \lambda_x & 0 & 0 \\ 0 & 1 & 0 \\ 0 & 0 & \frac{1}{\lambda_x} \end{bmatrix}$$

$$[\mathbf{V}]_{xyz} = \begin{bmatrix} \dot{\epsilon}_x & 0 & 0 \\ 0 & 0 & 0 \\ 0 & 0 & -\dot{\epsilon}_x \end{bmatrix}$$

being \mathbf{F}_D the right tensor of the deformation gradient. As can be seen from the following image (Fig. 3), relative to the circumferences of Mohr for the strain rate \mathbf{V} , at each instant of the test, the strain occurs in pure shear mode.

The deformation in the z -direction is free, therefore in the absence of external loads in this direction is not generated stress ($\sigma_z = 0$). Moreover, from the generalized Hooke's law $\dot{\epsilon}_y = \dot{\sigma}_y - \nu(\dot{\sigma}_x + \dot{\sigma}_z)$, being for incompressible materials $\nu = 1/2$ [3], for the y -direction stress is $\dot{\sigma}_y = \nu \dot{\sigma}_x = \dot{\sigma}_x/2$. In conclusion, during the planar test, the stress tensor \mathbf{T} follows the variation equation

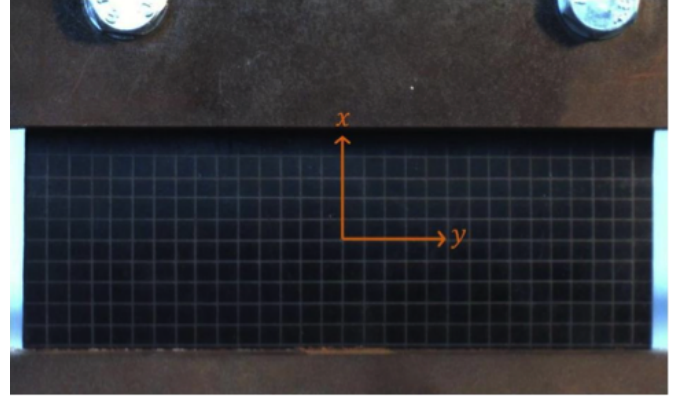


Fig. 1. Reference system, x-y plane

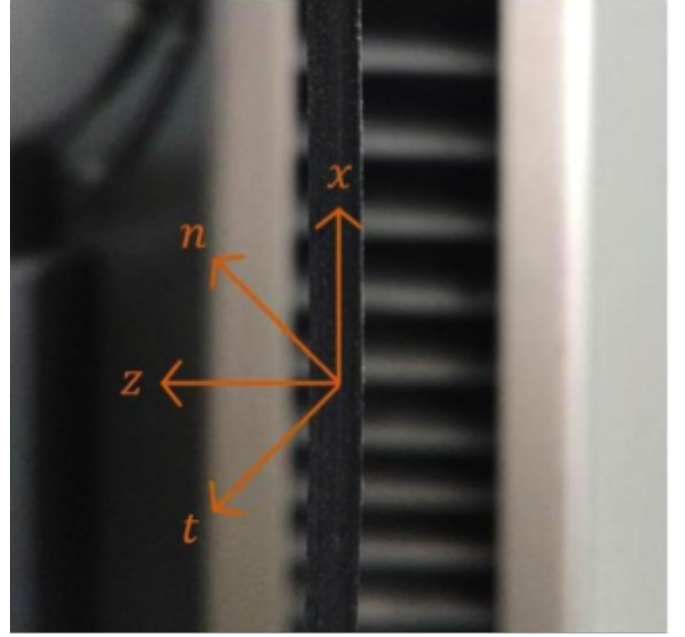


Fig. 2. Reference system, x-z plane

$$\left[\frac{d\mathbf{T}}{dt} \right]_{xyz} = \begin{bmatrix} \dot{\sigma}_x & 0 & 0 \\ 0 & \frac{\dot{\sigma}_x}{2} & 0 \\ 0 & 0 & 0 \end{bmatrix}$$

Unlike from strain, a condition of pure shear not realized for stress. However, the deviator stress tensor \mathbf{T}' still takes a pure shear connotation (see Fig. 4):

$$\left[\frac{d\mathbf{T}'}{dt} \right]_{xyz} = \begin{bmatrix} \frac{\dot{\sigma}_x}{2} & 0 & 0 \\ 0 & 0 & 0 \\ 0 & 0 & -\frac{\dot{\sigma}_x}{2} \end{bmatrix}$$

n and t are the orthogonal directions to the y -axis and forming angles of 45° with the x - and z -axis (Fig. 2). Since $\dot{\tau}_{nt} = \dot{\sigma}_x/2$, and being $\dot{\gamma}_{nt} = 2\dot{\epsilon}_x$, the calculation of the shear modulus G is carried out using the formula

$$G = \frac{d\tau_{nt}}{d\gamma_{nt}} = \frac{1}{4} \frac{d\sigma_x}{d\epsilon_x}$$

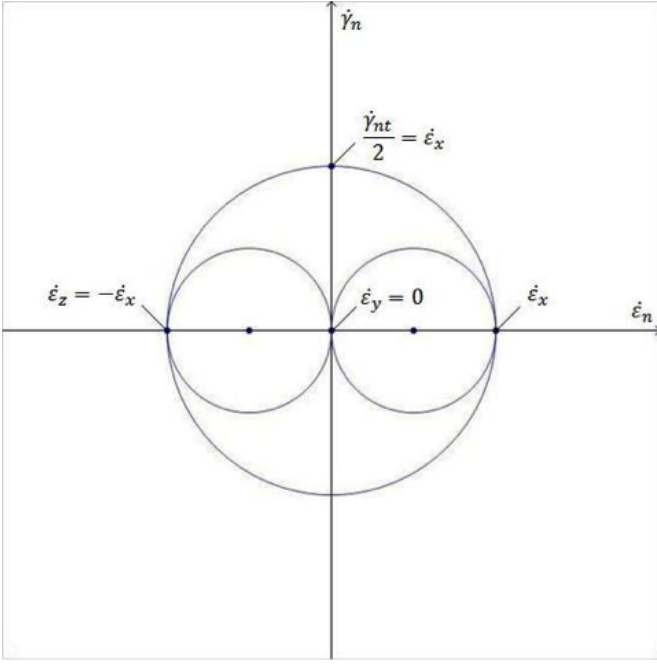


Fig. 3. Circumferences of Mohr of the strain rate tensor.

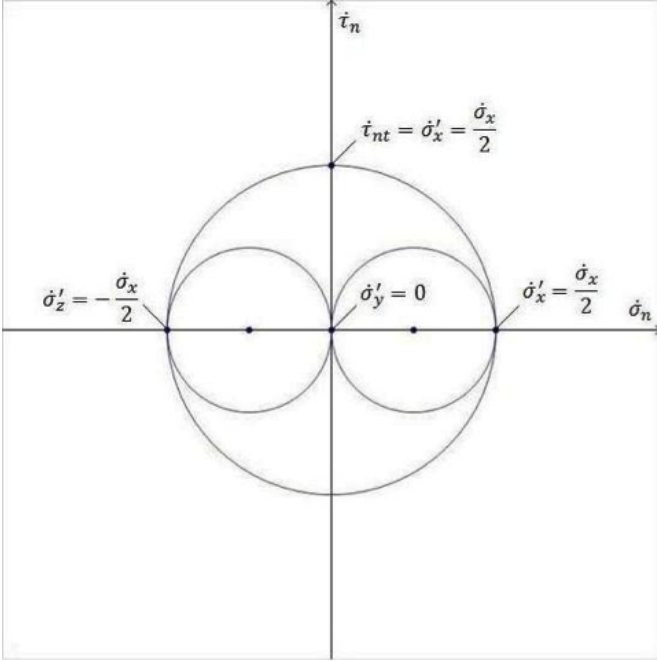


Fig. 4. Circumferences of Mohr of the stress rate deviator tensor.

IV. EXPERIMENTAL TESTS

The tested material is SBR filled with 25% of carbon black. The tests were performed on specimens cut from a sheet having a 3 mm thickness. These were carried out with a test machine Zwick/Roel, model Z100, equipped with 1 kN load cell, to imposed deformation, while maintaining constant the speed of the movable crossbar.

The uniaxial tests were performed on rectangular specimens,

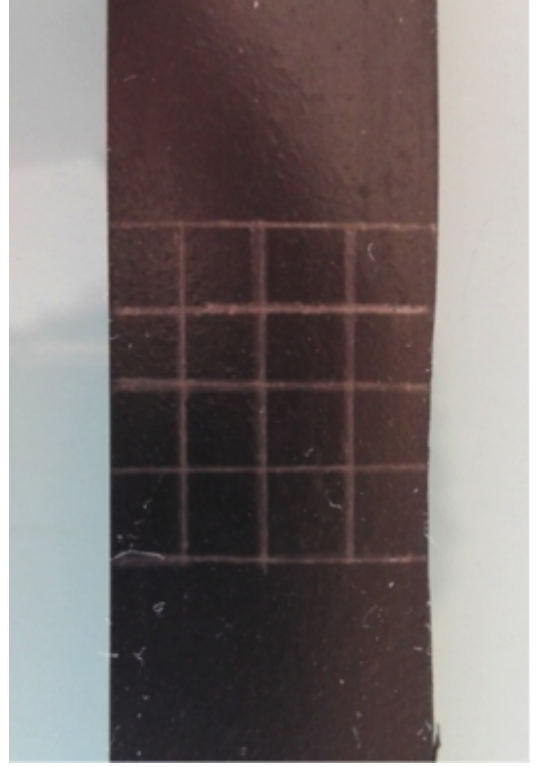


Fig. 5. Grid for the optical relief of the strain.

20 mm wide and 180 mm long, with a gauge length of 120 mm.

In the planar tests, was adopted a rectangular specimen, 150 mm wide and 70 mm long, having a gauge length of 50 mm.

For the measurement of deformations of the specimen was adopted an optical method. In effect, the large deformations do not allow easy application of the classic method of the strain gages. The used solution is based on tracing a grid on the specimen surface, which allows to highlight the location of certain specific points. By known distances between various points of the grid in the absence of load, just evaluate their new position for load applied to achieve the deformation.

For image acquisition, carried out at a constant rate, it used a digital camera Basler acA1300-30gm. It is equipped with a Sony CCD sensor ICX445 that provides 8-bit greyscale images at a maximum frame rate of 30 per second, with a resolution of 1280x960 px.

To provide an accurate strain measurement, the Vision Builder AI software of National Instruments acquires and processes images through the Vision Assistant command. At first a *convolution filter* is applied to emphasize the grid. In fact, the alteration of the grid, caused by the specimen stretching, reduces the brightness and thus the contrast with the background, making difficult the identification of the points by the software [33]. Finally, a *median filter* removes the image residual noise.



Fig. 6. Uniaxial Test Setup.

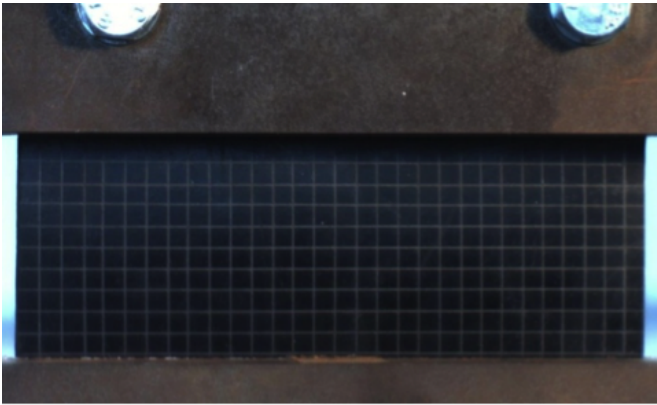


Fig. 7. Not processed image.

V. RESULTS

By the stress and strain values, the relationships of various functional dependencies between the physical quantities involved is obtained. The storage modulus were determined from the mathematical derivation of these functions.

The uniaxial testing allows to express both the normal stress as a function of the normal strain in the vertical direction (loading direction), and the normal strain in the horizontal direction (orthogonal to the loading direction) as a function of vertical strain. From the first of these applications the normal storage modulus $E = d\sigma/d\varepsilon_\nu$ [24] is obtained, from the second application the transverse contraction coefficient $\nu = -d\varepsilon_o/d\varepsilon_\nu$.

As already verified during a previous study on a silicone, developed at the University of Catania [25], a small strain rate, lower than ASTM standards, could rise viscoelastic relaxation phenomena in elastomers (decreasing of stress level compared to the strain achieved). Increasing the execution test rate, this aspect can be kept under control, drastically mitigating the effects. As a consequence of this, the stress-strain curve is higher for the higher test rate, then the rubber manifests an increase of stiffness and mechanical resistance

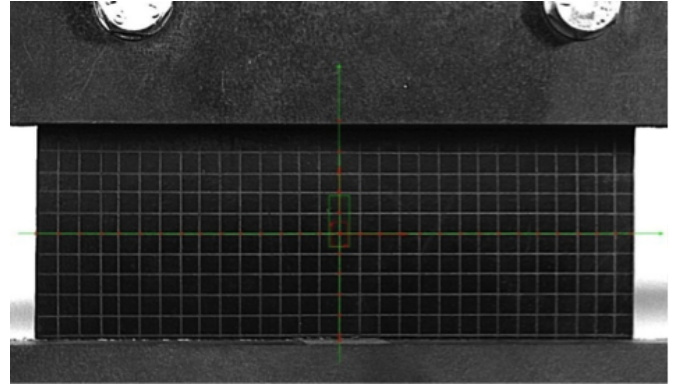


Fig. 8. Localization of points on the processed image.

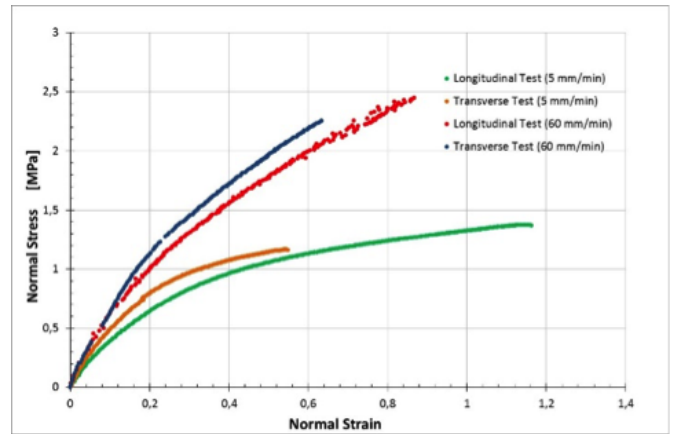


Fig. 9. Uniaxial Test: Normal Stress vs Normal Strain.

to the growing of the test speed. A decrease of the failure strain is associated. It also occurs a different location of the sample crack, depending on the execution test rate. At the ends, near the gripping point, for tests with crossbar that moves 5 mm/min; at the center of the specimen for the tests with speed of 60 mm/min.

In all performed tests, the value of Young's modulus E at the $O(0,0)$ ranged between 6.45 and 7.70 MPa, comparable with values reported in the literature for PDMS filled by carbon black (25%) [34]. The stretching at failure is much lower than the average obtained in the styrene-butadiene rubber [34].

In addition, at the $O(0,0)$, the Poisson's ratio ν is greater for the high-speed tests (0.460 and 0.490) compared to those at low speed (0.360 and 0.387). For the same rate of the crossbar, instead, the tested elastomer shows a greater Young's modulus and Poisson's ratio in the transverse test, but a lesser failure strain. It is interesting to observe that for faster tests the coefficient ν , evaluated by means of real strains, assumes constant value and close to the theoretical limit value of 0.5, maximum value for isotropic materials [26], which characterizes the incompressibility, during the entire test. This statement is true only for the Hencky's tensor. Adopting instead other tensors of deformation, it decreases during the experimental test, being equal to about 0.5 only at the beginning of the test

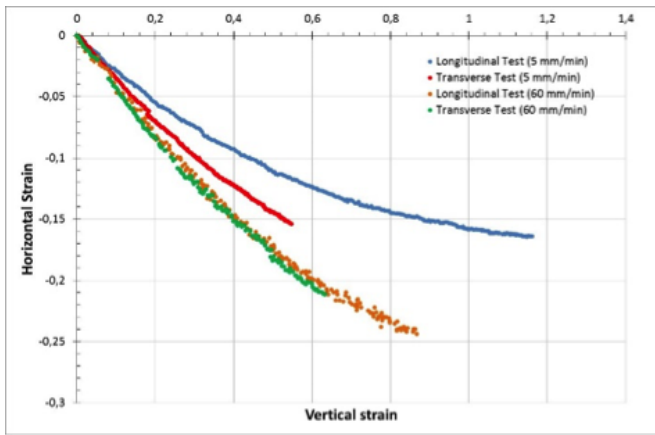


Fig. 10. Uniaxial Test: Horizontal Strain vs Vertical Strain.

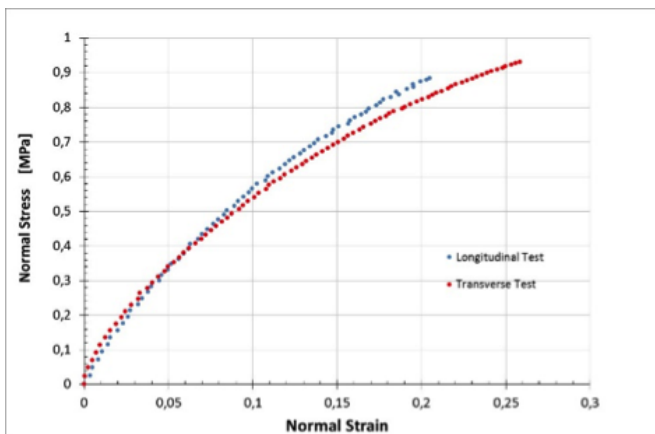


Fig. 11. Planar Test: Normal Stress vs Normal Strain.

and reaching to several lower values for large deformations [8]. The shear modulus $G = \frac{d\tau}{d\gamma} = (d\sigma_x)/(d\varepsilon_x)/4$ is calculated based on information extracted in the planar test.

From the analysis carried out, the module G at the origin is 2.04 MPa for longitudinal test and 1.94 MPa for the transverse direction to the calendaring.

For each curve a high correlation coefficient value, greater than 0.995, has achieved, demonstrating the low-degree polynomial expressions are well suited to describing the relationships between the treated physical quantities [35], [36]. In uniaxial test, the horizontal-vertical true strain function is well represented by a linear expression. Instead, the appropriate polynomial relationship in order to describe the trend of the stress as a function of vertical strain is of 4th order, both in uniaxial and planar tensile tests.

VI. CONCLUSION

The uniaxial and planar tensile tests on specimens of SBR filled with carbon black are carried out.

Due to the high deformability, the material under stress, undergoes marked deformation. In these circumstances the classical methods of measuring deformation fall in default and require alternative assessment criteria which take into

account the highly hyperelastic material characteristics. Then, they applied optical methods for overcoming this limit to characterize the elastomer.

The collected data were analyzed to determine the main elastomer storage modules. Different responses in relation to the different direction of load application are obtained, studying anisotropy expressed by the material due to the production process of calendaring elastomeric sheet. Given the high variability of the materials properties, the results were compared with those indicated in the literature for the styrene-butadiene rubber filled with carbon black. The normal storage modulus (stiffness) and the transverse contraction coefficient (Poisson's ratio) of the SBR as a function of the filler percentage have appeared, in accordance with the data available, lower for the tests with load applied in the calendaring direction.

REFERENCES

- [1] W. F. Smith and J. Hashemi, *Foundations of materials science and engineering*. McGraw-Hill, 2011.
- [2] P. Cheremisinoff, *Handbook of engineering polymeric materials*. CRC Press, 1997.
- [3] L. R. G. Treloar, *The physics of rubber elasticity*. Oxford University Press, USA, 1975.
- [4] S. Kawabata, Y. Yamashita, H. Ooyama, and S. Yoshida, "Mechanism of carbon-black reinforcement of rubber vulcanizate," *Rubber Chemistry and Technology*, vol. 68, no. 2, pp. 311–329, 1995.
- [5] P. Kundu, "Improvement of filler-rubber interaction by the coupling action of vegetable oil in carbon black reinforced rubber," *Journal of applied polymer science*, vol. 75, no. 6, pp. 735–739, 2000.
- [6] G. La Rosa and F. L. Savio, "A first approach to the experimental study of fracture parameters in opening and mixed mode by caustics," *Procedia Engineering*, vol. 109, pp. 418–426, 2015.
- [7] G. Cannistraro, M. Cannistraro, A. Cannistraro, A. Galvagno, and G. Trovato, "Evaluation on the convenience of a citizen service district heating for residential use. a new scenario introduced by high efficiency energy systems," *International Journal of Heat and Technology*, vol. 33, no. 4, pp. 167–172, 2015.
- [8] S. Brusca, R. Lanzafame, and M. Messina, "Design and performance of a straight-bladed darrieus wind turbine," *International Journal of Applied Engineering Research*, vol. 10, no. 16, pp. 37 431–37 438, 2015.
- [9] M. Cali, S. M. Oliveri, G. Sequenzia, and G. Fatuzzo, "An effective model for the sliding contact forces in a multibody environment," in *Advances on Mechanics, Design Engineering and Manufacturing*. Springer, 2017, pp. 675–685.
- [10] M. Cali, D. Speranza, and M. Martorelli, "Dynamic spinnaker performance through digital photogrammetry, numerical analysis and experimental tests," in *Advances on Mechanics, Design Engineering and Manufacturing*. Springer, 2017, pp. 585–595.
- [11] F. Cataldo, O. Ursini, and G. Angelini, "Biodiesel as a plasticizer of a sbr-based tire tread formulation," *ISRN Polymer Science*, vol. 2013, 2013.
- [12] G. La Rosa, C. Clienti, and F. Lo Savio, "Fatigue analysis by acoustic emission and thermographic techniques," *Procedia Engineering*, vol. 74, pp. 261–268, 2014.
- [13] S. Brusca, F. Famoso, R. Lanzafame, S. Mauro, A. Garrano, and P. Monforte, "Theoretical and experimental study of gaussian plume model in small scale system," vol. 101, 2016, pp. 58–65.
- [14] E. Pedulla, F. L. Savio, G. Plotino, N. M. Grande, S. Rapisarda, G. Gambarini, and G. La Rosa, "Effect of cyclic torsional preloading on cyclic fatigue resistance of protaper next and mtwo nickel-titanium instruments," *Giornale Italiano di Endodonzia*, vol. 29, no. 1, pp. 3–8, 2015.
- [15] E. Pedullà, F. L. Savio, S. Boninelli, G. Plotino, N. M. Grande, G. La Rosa, and E. Rapisarda, "Torsional and cyclic fatigue resistance of a new nickel-titanium instrument manufactured by electrical discharge machining," *Journal of endodontics*, vol. 42, no. 1, pp. 156–159, 2016.

- [16] G. Cannistraro, M. Cannistraro, A. Cannistraro, A. Galvagno, and G. Trovato, "Reducing the demand of energy cooling in the ced, "centers of processing data", with use of free-cooling systems," *International Journal of Heat and Technology*, vol. 34, no. 3, pp. 498–502, 2016.
- [17] M. Cali, G. Sequenzia, S. Oliveri, and G. Fatuzzo, "Meshing angles evaluation of silent chain drive by numerical analysis and experimental test," *Meccanica*, vol. 51, no. 3, pp. 475–489, 2016.
- [18] M. Shahzad, A. Kamran, M. Z. Siddiqui, and M. Farhan, "Mechanical characterization and fe modelling of a hyperelastic material," *Materials Research*, vol. 18, no. 5, pp. 918–924, 2015.
- [19] D. Moreira and L. Nunes, "Comparison of simple and pure shear for an incompressible isotropic hyperelastic material under large deformation," *Polymer Testing*, vol. 32, no. 2, pp. 240–248, 2013.
- [20] J. Diani, M. Brieu, J.-M. Vacherand, and A. Rezgui, "Directional model for isotropic and anisotropic hyperelastic rubber-like materials," *Mechanics of Materials*, vol. 36, no. 4, pp. 313–321, 2004.
- [21] M. Cali and F. L. Savio, "Accurate 3d reconstruction of a rubber membrane inflated during a bulge test to evaluate anisotropy," in *Advances on Mechanics, Design Engineering and Manufacturing*. Springer, 2017, pp. 1221–1231.
- [22] F. Famoso, R. Lanzafame, S. Maenza, and P. Scandura, "Performance comparison between micro-inverter and string-inverter photovoltaic systems," vol. 81, 2015, pp. 526–539.
- [23] M. Cali, S. M. Oliveri, G. Fatuzzo, and G. Sequenzia, "Error control in uav image acquisitions for 3d reconstruction of extensive architectures," in *Advances on Mechanics, Design Engineering and Manufacturing*. Springer, 2017, pp. 1209–1219.
- [24] O. Starkova and A. Aniskevich, "Poisson's ratio and the incompressibility relation for various strain measures with the example of a silica-filled sbr rubber in uniaxial tension tests," *Polymer Testing*, vol. 29, no. 3, pp. 310–318, 2010.
- [25] G. Basile, "Analisi teorico sperimentale di materiali iperelastici," 2012.
- [26] R. W. Ogden, *Non-linear elastic deformations*. Courier Corporation, 1997.
- [27] W. Schneider, F. Huybrechts, and K. Nordsiek, "Process oils in oil extended sbr," *Kautschuk und Gummi, Kunststoffe*, vol. 44, no. 6, pp. 528–536, 1991.
- [28] M. Wozniak, C. Napoli, E. Tramontana, G. Capizzi, G. L. Sciuto, R. K. Nowicki, and J. T. Starczewski, "A multiscale image compressor with rbfnn and discrete wavelet decomposition," in *International Joint Conference on Neural Networks (IJCNN)*. IEEE, 2015, pp. 1–7.
- [29] C. Napoli, G. Pappalardo, and E. Tramontana, "An agent-driven semantical identifier using radial basis neural networks and reinforcement learning," in *Proceedings of the XV Workshop Dagli Oggetti agli Agenti*, vol. 1260. CEUR-WS, 2014. [Online]. Available: <http://ceur-ws.org/Vol-1260/>
- [30] C. Napoli and E. Tramontana, "An object-oriented neural network toolbox based on design patterns," in *International Conference on Information and Software Technologies*. Springer International Publishing, 2015, pp. 388–399.
- [31] M. Wozniak, D. Polap, G. Borowik, and C. Napoli, "A first attempt to cloud-based user verification in distributed system," in *Asia-Pacific Conference on Computer Aided System Engineering (APCASE)*. IEEE, 2015, pp. 226–231.
- [32] C. Napoli and E. Tramontana, "Massively parallel wrnn reconstructors for spectrum recovery in astronomical photometrical surveys," *Neural Networks*, vol. 83, pp. 42–50, 2016.
- [33] G. Capizzi, G. L. Sciuto, C. Napoli, E. Tramontana, and M. Woniak, "Automatic classification of fruit defects based on co-occurrence matrix and neural networks," in *2015 Federated Conference on Computer Science and Information Systems (FedCSIS)*, Sept 2015, pp. 861–867.
- [34] J. Han, X. Zhang, W. Guo, and C. Wu, "Effect of modified carbon black on the filler–elastomer interaction and dynamic mechanical properties of sbr vulcanizates," *Journal of applied polymer science*, vol. 100, no. 5, pp. 3707–3712, 2006.
- [35] F. Bonanno, G. Capizzi, S. Coco, A. Laudani, and G. L. Sciuto, "A coupled design optimization methodology for li-ion batteries in electric vehicle applications based on fem and neural networks," in *2014 International Symposium on Power Electronics, Electrical Drives, Automation and Motion*, June 2014, pp. 146–153.
- [36] F. Bonanno, G. Capizzi, and G. L. Sciuto, "A neuro wavelet-based approach for short-term load forecasting in integrated generation systems," in *2013 International Conference on Clean Electrical Power (ICCEP)*, June 2013, pp. 772–776.